56--02
117229
19?

UPWIND RELAXATION ALGORITHMS
FOR EULER/NAVIER-STOKES EQUATIONS

J. L. Thomas
R. W. Walters
D. H. Rudy
R. C. Swanson
NASA Langley Research Center
Hampton, Virginia

C-2

Abstract

The present paper will present a description of and results from a new solution algorithm for the compressible Navier-Stokes equations developed by a team of researchers at Langley Research Center. The main features of the algorithm are second- or third-order accurate upwind discretization of the convective and pressure derivatives and a relaxation scheme for the unfactored implicit backward Euler time method, implemented in a finite-volume formulation.

Upwind methods have been successfully used to obtain solutions to the Euler equations for flows with strong shock waves. One reason for this success is that these methods directly simulate the signal propagation features of hyperbolic equations. Furthermore, these methods have the advantage of being naturally dissipative. Upwind differencing has been used for the pressure and convective terms in the present Navier-Stokes algorithm while central differencing has been used for the viscous terms. The particular upwind method being used is based on the flux-vector-splitting technique developed by Van Leer (ref. 1) and both second- and third-order accurate discretizations have been developed.

Currently, the most widely used implicit solution techniques for the Navier-Stokes equations use approximate factorization (AF) methods to treat multi-dimensional problems. Although the implicit AF methods are unconditionally stable in two dimensions, they require an optimal set of iteration parameters, which are difficult to obtain, for rapid convergence. Furthermore, the implicit AF schemes are only conditionally stable for the three-dimensional Navier-Stokes equations. However, the upwind discretization leads to a diagonally dominant matrix structure which allows large time steps to be taken in multi-dimensional problems. The time integration scheme being used in the present algorithm corresponds to a line Gauss-Seidel relaxation method. This method produces good convergence rates for steady-state flows, and most of the algorithm has been vectorized on the NASA Langley VPS 32 computer.

The Navier-Stokes algorithm has been tested for several two-dimensional flow problems such as the laminar boundary layer flow on a flat plate and the flow produced by an oblique shock wave impinging on a laminar boundary layer developing on a flat plate. Solutions for both problems gave excellent results which are presented in this paper. Present effort is directed toward the extension of the scheme to the full three-dimensional Navier-Stokes equations.

90

Upwind Relaxation Algorithms for the
Euler/Navier-Stokes Equations

The purpose of this paper is to present upwind relaxation algorithms for accurate and reliable steady-state solutions to either the compressible Euler (inviscid) or Navier-Stokes (viscous) equations. The main feature of the algorithms is the use of second- or third-order accurate upwind discretizations of the convective and pressure terms, which enables implicit line relaxation strategies to be developed for rapid solutions to the steady-state equations. The basic algorithm for three-dimensional flows is discussed. Both inviscid and viscous (using thin-layer Navier-Stokes approximations) computations are shown for a series of two-dimensional flows.

The relaxation algorithm for the time-dependent Euler equations written in conservation form and generalized coordinates is shown. The equation to be solved with relaxation corresponds to the linearized, backward-time approximation in delta form. The inviscid flux is split according to the eigenvalues of the characteristic equation, which recognizes the signal propagation features of the hyperbolic equations and enables relaxation approaches to be exploited for solutions to the steady-state equations. The particular flux splitting technique used corresponds to that developed by Van Leer (ref. 1), although the advantages resulting from upwind differencing would apply equally as well to other splitting techniques. Applying upwind differencing in the streamwise (ξ) direction on the implicit (left-hand) side of the equation in delta form leaves an equation to be solved in the cross flow (η-ζ) plane. The streamwise relaxation is effected by sweeping in the ξ-direction through the mesh, alternating the direction of the sweep every other pass in order to maintain stability for higher order differencing.

Non-linear updating of the residual is indicated, corresponding to upstream cross-flow planes evaluated at time level n+1 when sweeping from upstream to downstream, and vice-versa. The upwind relaxation scheme indicated is unconditionally stable and maximal damping occurs at large time steps. This is in contrast to approximately factored approaches, which require an optimal set of iteration parameters, which are difficult and time consuming to obtain, for rapid convergence. The relaxation scheme also has the advantage that it recovers conventional space marching techniques for supersonic flows in the ξ-direction.

Time-dependent Euler equations in generalized coordinates

$$\frac{\partial \hat{Q}}{\partial \tau} + \frac{\partial \hat{F}}{\partial \xi} + \frac{\partial \hat{G}}{\partial \eta} + \frac{\partial \hat{H}}{\partial \zeta} = 0$$

Linearized implicit time integration

$$\left[\frac{I}{J \Delta \tau} + \delta_\xi \frac{\partial \hat{F}}{\partial Q} + \delta_\eta \frac{\partial \hat{G}}{\partial Q} + \delta_\zeta \frac{\partial \hat{H}}{\partial Q} \right] \Delta Q = -R^n$$

Applying upwind relaxation in the streamwise (ξ) direction leaves an equation to be solved in the cross-flow (η-ζ) plane

$$\left[M + \delta_\eta \frac{\partial \hat{G}}{\partial Q} + \delta_\zeta \frac{\partial \hat{H}}{\partial Q} \right] \Delta Q = -R(Q^n, Q^{n+1})$$

Where

$$M = \frac{I}{J \Delta \tau} + \frac{\partial F^+}{\partial Q} - \frac{\partial F^-}{\partial Q} \qquad \Delta Q = Q^{n+1} - Q^n$$

The upwind differenced equation in the cross-flow plane can be solved using either relaxation or approximate factorization. The upwind relaxation shown corresponds to alternate line Gauss-Seidel sweeping with nonlinear updating of the residual indicated, although in practice the residual is updated linearly using the Jacobian matrices from the implicit side of the equation. With first-order implicit upwind differencing, either approach leads to two sweeps across the plane, solving a system of tridiagonal equations on each line. With relaxation in the cross-flow plane, the scheme is unconditionally stable for the linear wave equation and maximum damping occurs with large time steps. However, because the algorithm is recursive in nature, it cannot be completely vectorized on current pipeline supercomputers such as the CDC CYBER 205. The time step is limited to obtain optimal convergence with the approximate factorization in the cross-flow plane, but the scheme is completely vectorizable. Thus, a tradeoff exists between convergence rate and computational rate in determining the most efficient strategy. Vectorizable relaxation strategies, such as checkerboard algorithms, lead to faster computational rates with slightly lower convergence rates, owing to the underrelaxation required for stability.

$$\left[M + \delta_\eta \frac{\partial \hat{G}}{\partial Q} + \delta_\zeta \frac{\partial \hat{H}}{\partial Q} \right] \Delta Q = -R(Q^n, Q^{n+1})$$

Upwind relaxation (Line Gauss-Seidel — alternate sweeping)

$$\left[M + \frac{\partial \hat{G}^+}{\partial Q} - \frac{\partial \hat{G}^-}{\partial Q} + \delta_\zeta \frac{\partial \hat{H}}{\partial Q} \right] \Delta Q = -R(Q^n, Q^{n+1}) \quad \zeta - \text{line implicit}$$

$$\left[M + \frac{\partial \hat{H}^+}{\partial Q} - \frac{\partial \hat{H}^-}{\partial Q} + \delta_\eta \frac{\partial \hat{G}}{\partial Q} \right] \Delta Q = -R(Q^n, Q^{n+1}) \quad \eta - \text{line implicit}$$

Approximate factorization

$$\left[M + \delta_\eta \frac{\partial \hat{G}}{\partial Q} \right] \left[M^{-1} \right] \left[M + \delta_\zeta \frac{\partial \hat{H}}{\partial Q} \right] \Delta Q = -R(Q^n, Q^{n+1})$$

The convective and pressure terms are split according to the flux vector splitting technique developed by Van Leer, which is implemented in a control-volume formulation. The flux difference is computed from the difference of split fluxes across all boundaries, where the upwinding is incorporated through an interpolation of conserved variables. A one-parameter family of interpolations is used. This family ranges from fully upwind second-order to upwind-biased third-order approximations. Viscous terms are differenced using second-order central differences, so that the method for viscous flows is limited currently to second order.

Upwind flux splitting for convective and pressure terms

$$\delta_\xi F = \delta_\xi^- F^+ + \delta_\xi^+ F^-$$

Where upwind differences effected through interpolation of conserved variables in terms of 1-parameter family

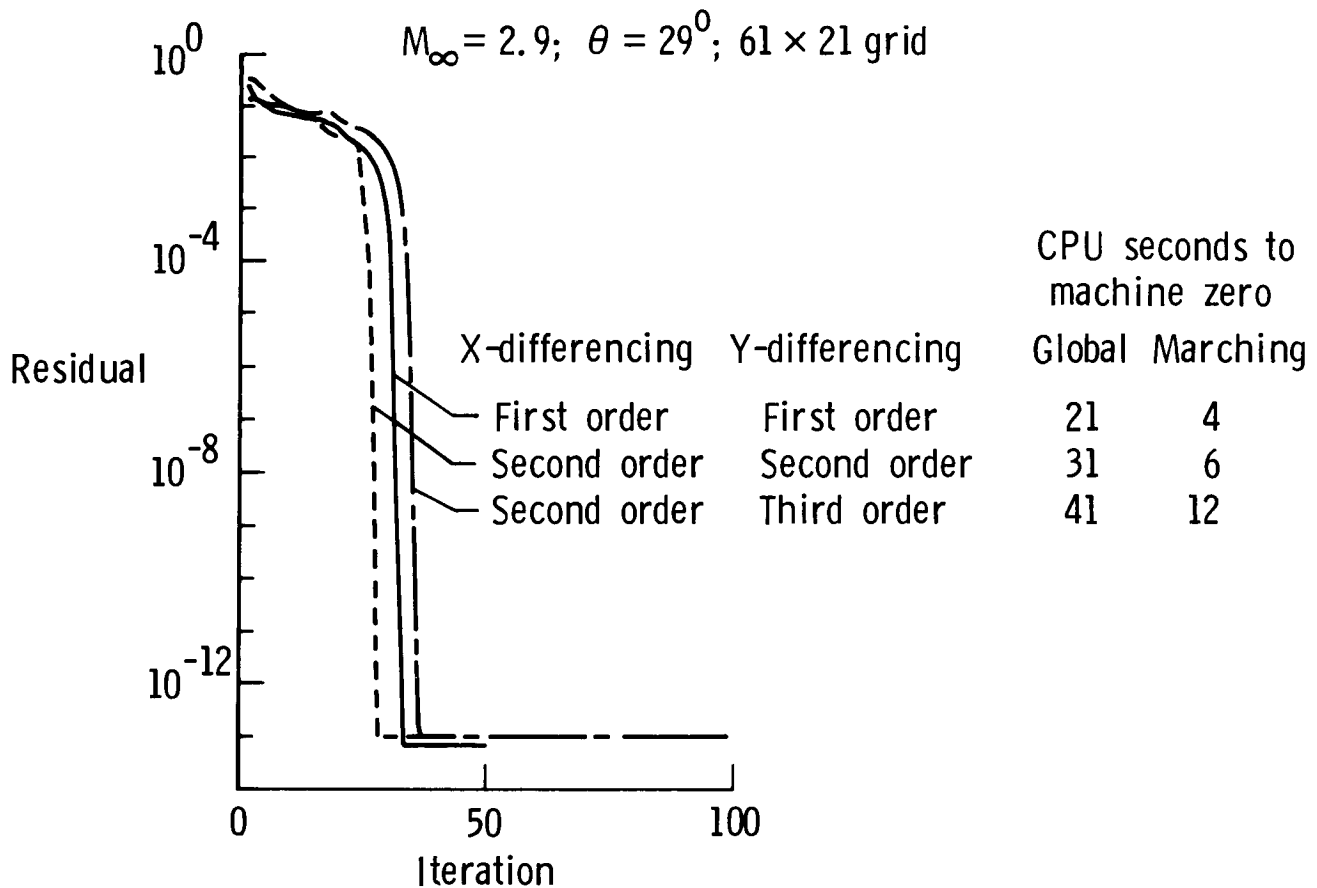$$\delta_\xi^- F^+ = F^+ (Q^-)_{i+\frac{1}{2}} - F^+ (Q^-)_{i-\frac{1}{2}}$$

$$Q^-_{i+\frac{1}{2}} = Q_i + \frac{1}{4} \left[(1-K)\nabla + (1+K)\Delta \right] Q_i$$

$$K = \begin{cases} -1 & \text{Second order fully upwind} \\ +1 & \text{Second order central difference} \\ 1/3 & \text{Third order upwind - biased} \end{cases}$$

Viscous terms differenced with second-order central differences
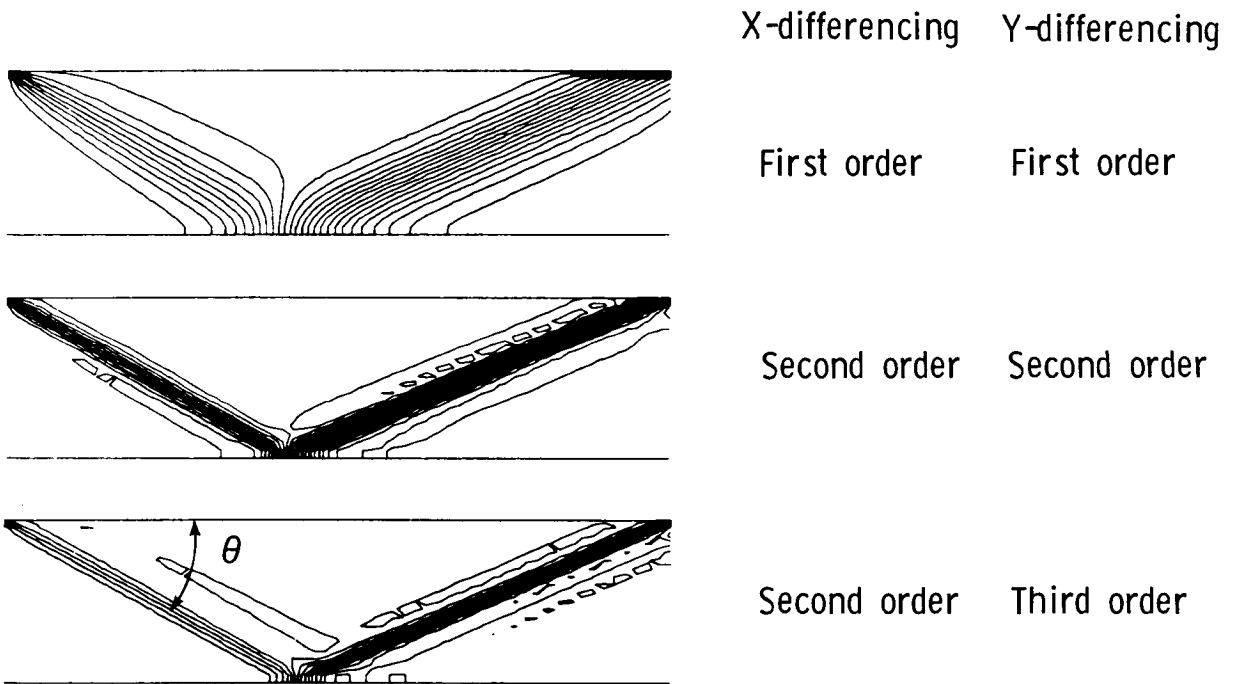
Inviscid Shock Reflection From Flat Plate

Application of the relaxation algorithm to the solution of an inviscid shock reflection from a flat surface is shown. The freestream Mach number is 2.9 and the shock angle is 29°. Fully upwind spatial differencing in the streamwise direction is used along with vertical Gauss-Seidel line relaxation; this leads to the quadratic convergence shown since the flow is fully supersonic. First-order differencing leads to block tridiagonal line inversions; second- or third-order differencing leads to block pentadiagonal line inversions. The residual history shown is for a global line relaxation strategy (sweeping downstream through the mesh). Further improvements in efficiency can be realized by removing linearization errors completely on a line before moving to the next line, and, thus, recovering a space marching method. The space marching strategy has also been extended to efficiently treat supersonic flows with embedded subsonic regions.

$M_\infty = 2.9$; $\theta = 29°$; 61 × 21 grid

X-differencing	Y-differencing	CPU seconds to machine zero	
		Global	Marching
First order	First order	21	4
Second order	Second order	31	6
Second order	Third order	41	12

Residual vs. Iteration (0 – 100)

Pressure contours for the inviscid shock reflection are shown with various orders of spatial differencing. The grid for each case is uniformly spaced in each of the two directions. The higher order methods are much less dissipative then the first-order scheme and show much higher resolution of the shock wave.

$$M_\infty = 2.9; \quad \theta = 29°; \quad 61 \times 21 \text{ grid}$$

	X-differencing	Y-differencing
	First order	First order
	Second order	Second order
	Second order	Third order

96

Residual Histories for First- and Second-Order Schemes

Residual histories for the transonic flow over a bump in a channel are shown. The incoming Mach number is 0.85, and a significant region of transonic flow exists as shown subsequently. The particular results shown were obtained with approximate factorization (AF) and with vertical line relaxation (LR) methods on a 34 × 18 H-mesh with uniform spacing. The Courant number for the LR scheme is on the order of 200, while that of the AF scheme is limited to 20. One iteration refers to two passes through the mesh using AF and one pass through the mesh using LR. The computational work per iteration on a scalar processor is roughly equal for the two methods and thus the LR scheme is much more efficient. On a vector processor, the computational rate per iteration for the LR scheme is two to three times slower than the AF scheme, even though more than 90 percent of the LR scheme has been vectorized. The only scalar operations in the LR scheme are the recursive forward-backward substitutions on a line; the lower-upper decomposition of the matrix equations is completely vectorizable. Thus, the relative efficiency of the two schemes depends on the type of computer on which the two approaches are implemented.

$M_\infty = 0.85$; $t/c = 4.2\%$; $h/c = 2.073$; 34 × 18 H-mesh
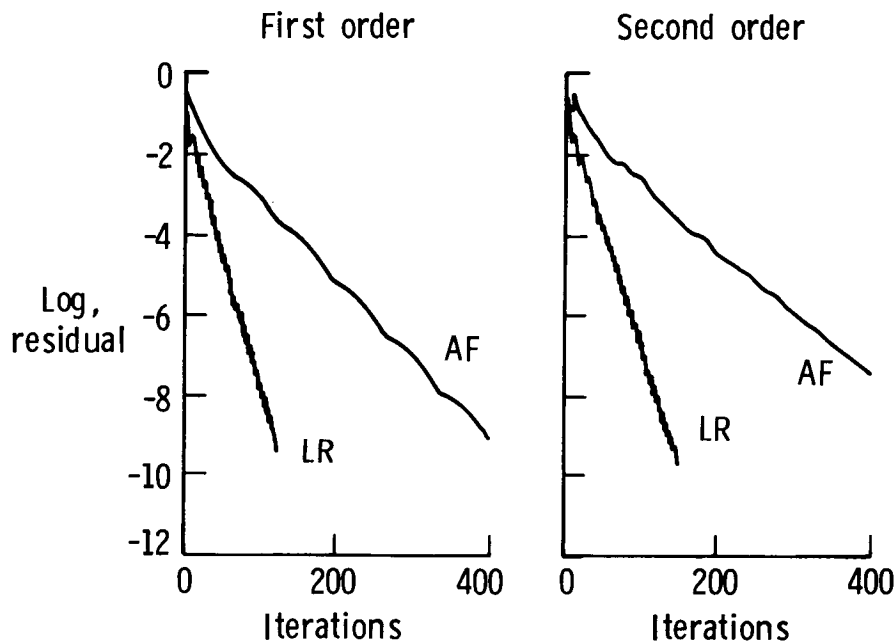
A computational grid for the transonic flow over a bump in a channel is shown. The thickness of the bump is 4.2 percent of the chord, and the channel is approximately two chords in height. The computational grid extends two chords ahead of and behind the bump and is clustered in the region near the bump. The grid is uniform in the vertical direction.

$h/c = 2.073$; $t/c = 4.2$ %; 85×41 H-mesh
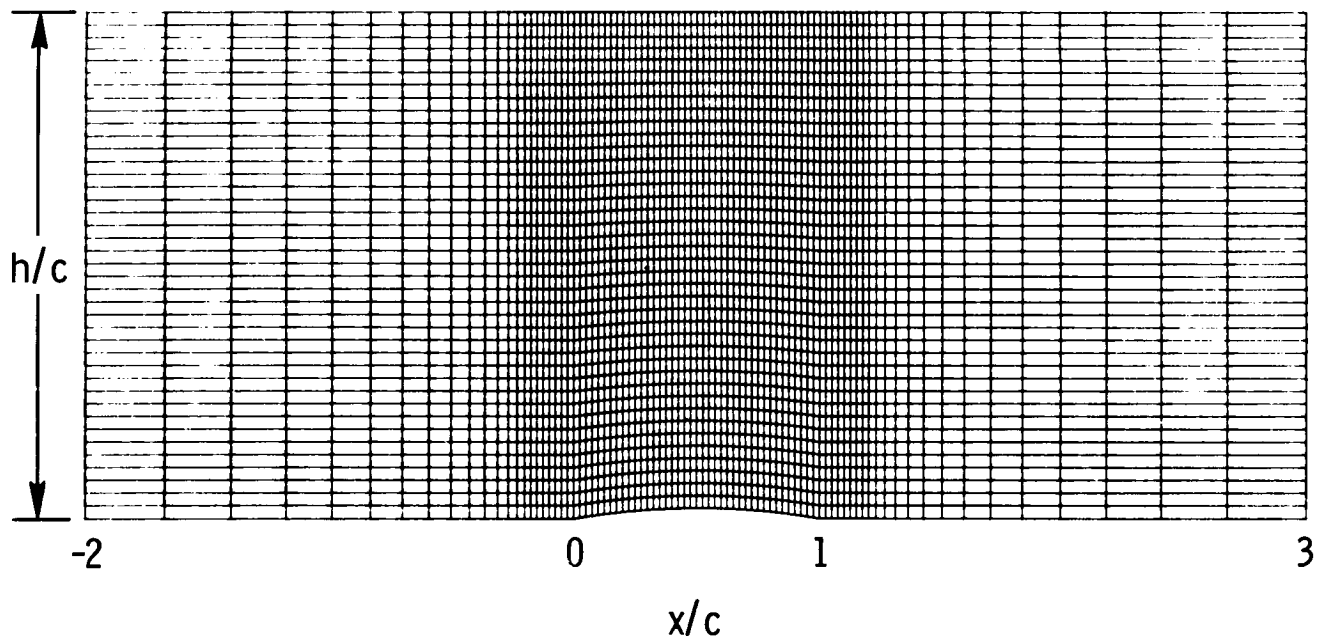
Pressure contours for the transonic flow over a bump in a channel obtained on the 85 × 41 computational grid are shown. A substantial region of transonic flow exists over the bump, and the shock is captured with two transition zones using the present method. The results shown were obtained with the fully upwind second-order scheme ($\kappa = -1$).

$$M_\infty = 0.85; \quad t/c = 4.2\%; \quad h/c = 2.073; \quad 85 \times 41 \, H\text{-mesh}$$
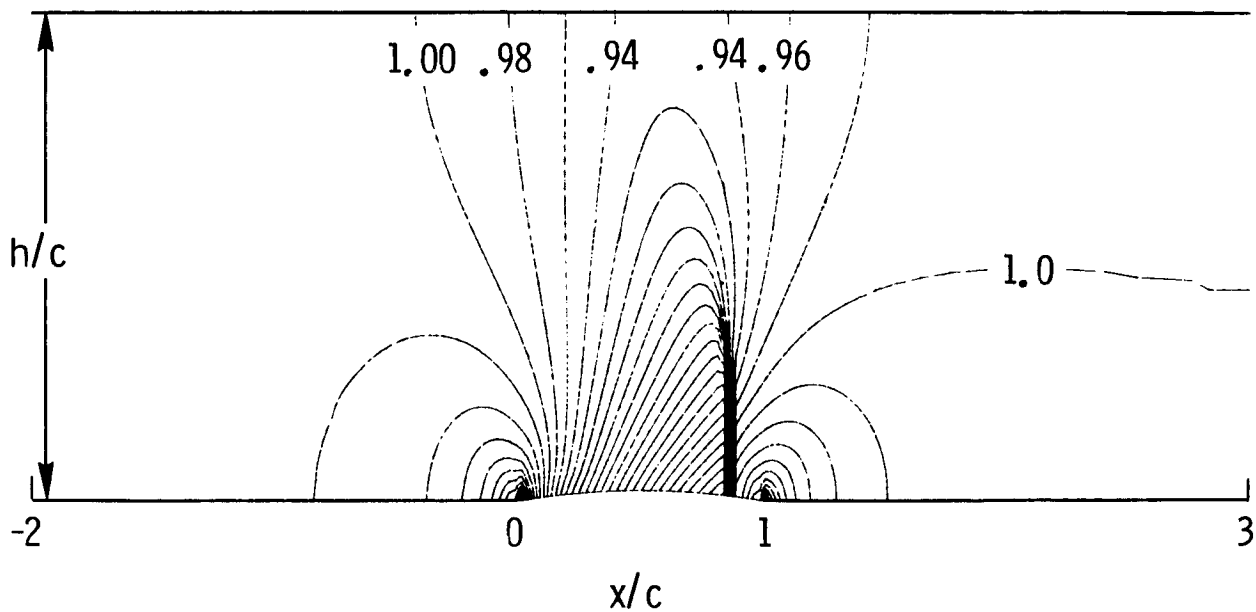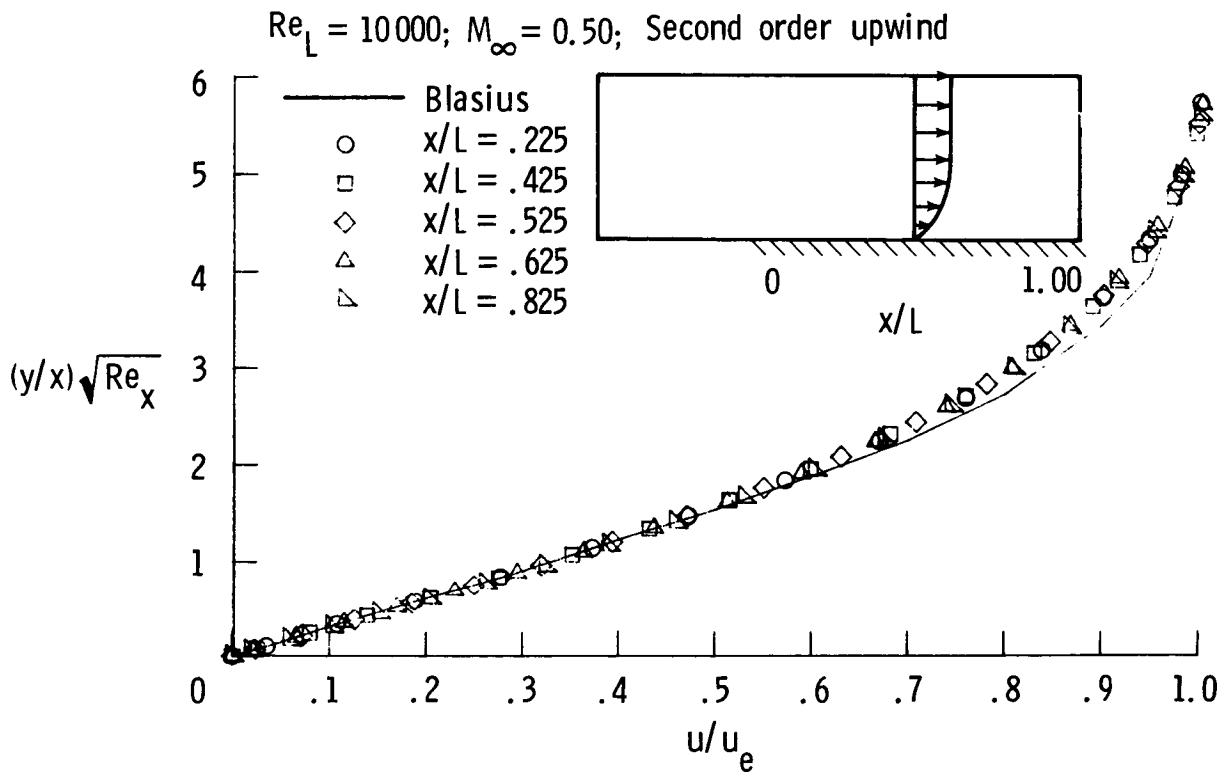
Applications of the relaxation algorithm to a series of viscous model problems
are shown. The first is one-dimensional Couette flow between a fixed lower plate and
a moving upper plate at low Reynolds number and Mach number. Velocity profiles ob-
tained with third-order upwind-biased differencing for the convective and pressure
terms and second-order central differencing for the viscous shear terms are shown
where the parameter B represents an applied pressure gradient term. No-slip velocity
and fixed-wall temperature boundary conditions were used. The relaxation method at
large time steps in one-dimension corresponds to Newton's method for finding
solutions to nonlinear systems of equations and convergence of the residual to
machine zero can be obtained in less than ten iterations. The computed velocity
profiles agree very closely with the exact result.

$$Re_H = 6.2; \quad M_0 = 0.09$$

—————— Exact solution

o Third order upwind-biased

B = -2   0   +7

y/H

u/u_0
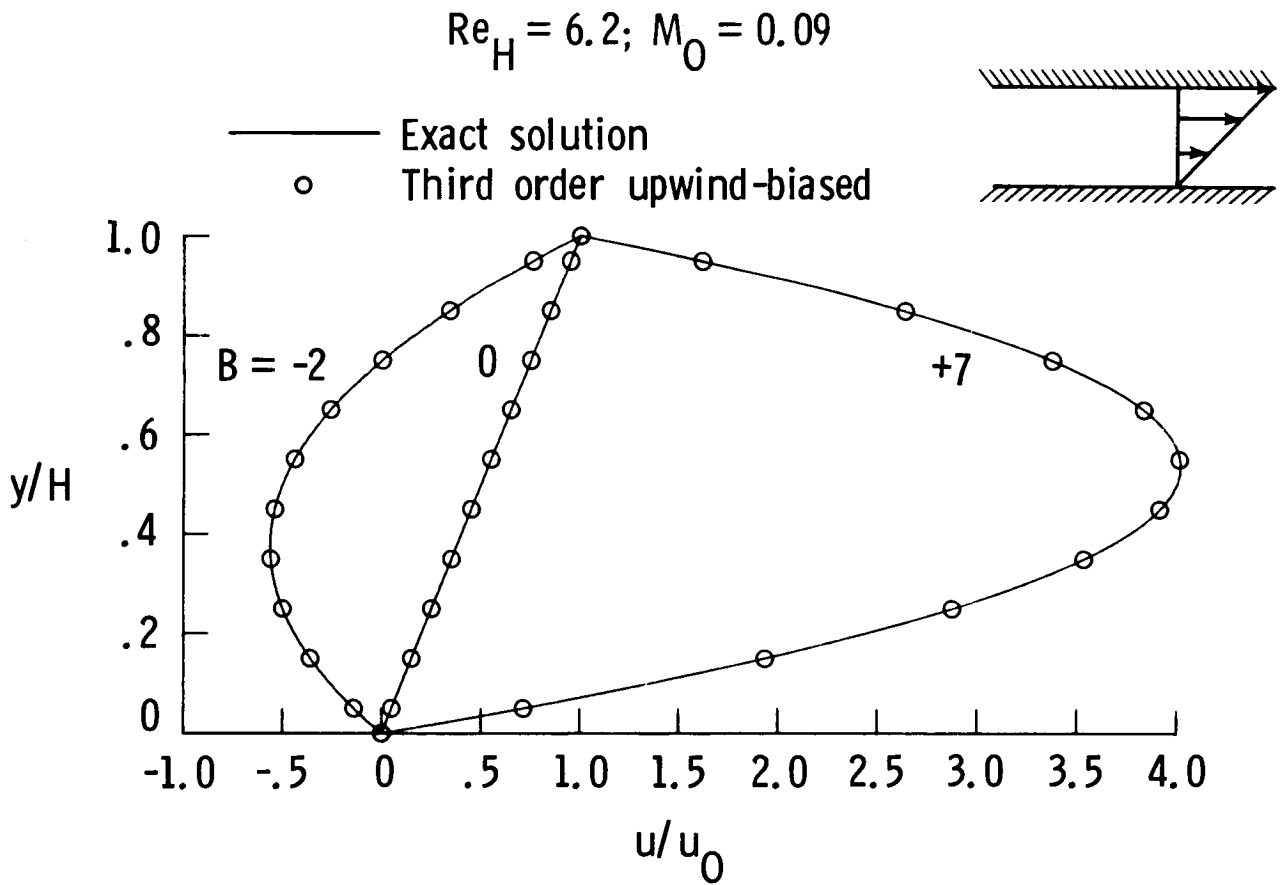
Flat-Plate Boundary Layer: Second-Order Differencing

The accurate computation of viscous effects with an upwind method is an important concern. Results are shown for the laminar flow over a flat plate using second-order ($\kappa = -1$) differencing for the pressure and convective terms. The freestream Mach number is 0.5 and the Reynolds number based on the length of the plate is 10,000. The results were obtained on a 30 × 40 computational grid, which is uniform in the streamwise direction and stretched in the direction normal to the plate. The computational domain is sketched; inflow conditions were applied upstream of the plate and outflow conditions above and downstream of the plate. No-slip, adiabatic wall conditions were specified on the plate. The computations recover the similarity velocity profiles, which develop very quickly downstream of the leading edge. The second-order scheme resolves the boundary layer adequately with approximately twenty points in the layer.


$Re_L = 10\,000$; $M_\infty = 0.50$; Second order upwind

Blasius
- ○ $x/L = .225$
- □ $x/L = .425$
- ◇ $x/L = .525$
- △ $x/L = .625$
- ◭ $x/L = .825$

$(y/x)\sqrt{Re_x}$

u/u_e

Results are shown using third-order upwind-biased differencing (κ = 1/3) for the convective and pressure terms. The accuracy relative to the second-order differencing is evident by comparison with the previous figure. The third-order differencing can be implemented with only a very small additional computational effort relative to the second-order scheme, since the computational molecule for both schemes only involves five points in any one direction. Central difference methods and the present upwind method are formally of the same order (second order) for viscous flows and one should expect roughly the same truncation error level. This has been verified in the present effort both analytically and numerically. In contrast, first-order upwind differencing leads to a boundary layer thickness four to five times that shown.

Re_L = 10000; M_∞ = 0.50; Third order upwind
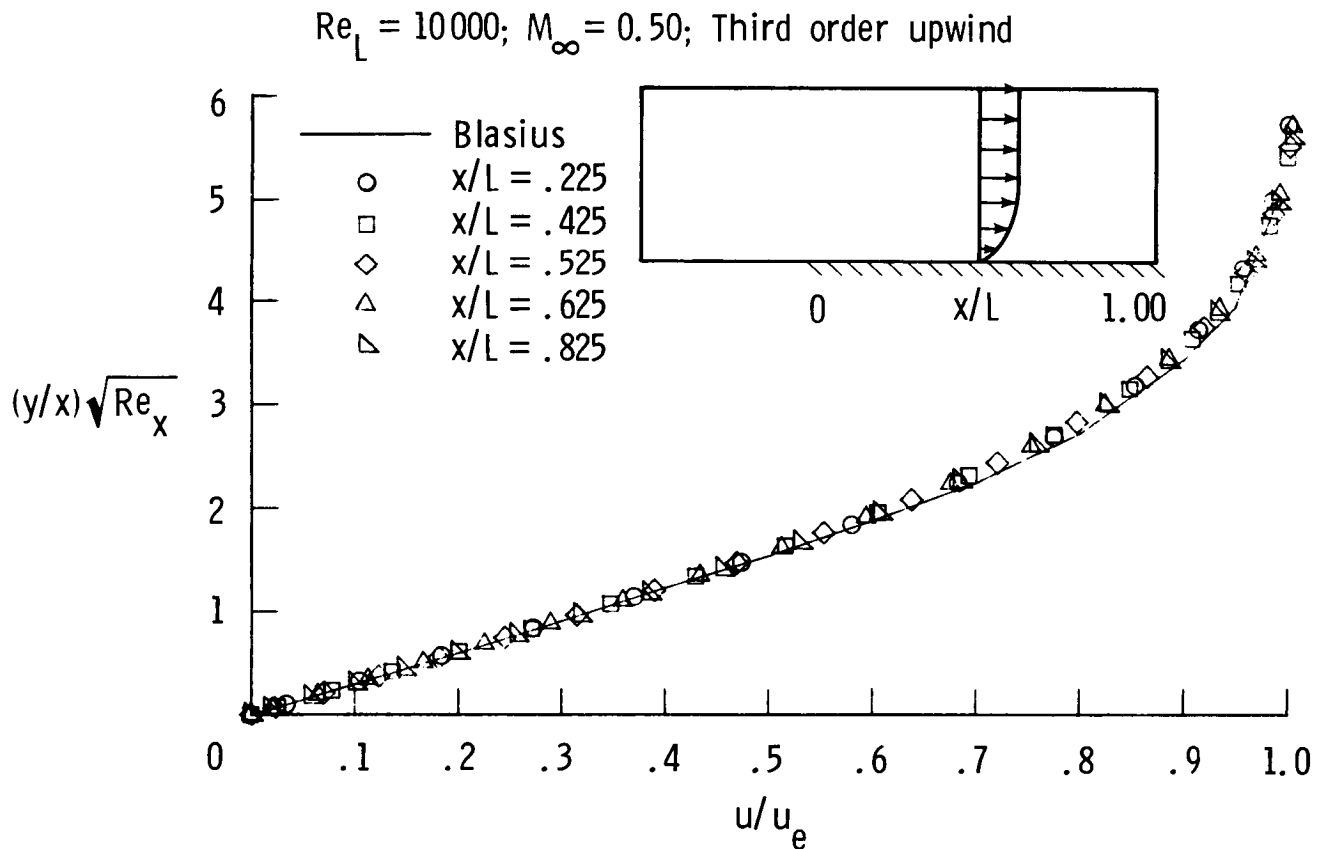
Shock-Boundary Layer Interaction

The final problem is that of an oblique shock wave impinging on a laminar boundary layer developing on a flat plate. The conditions correspond to the experiments of Hakkinen et al. (ref. 2) at a free-stream Mach number of 2.00 and a Reynolds number based on the length from the leading edge to the shock impingement point of 2.96×10^5. The shock is of sufficient strength to cause a separation of the developing laminar boundary layer, as evident in the computational results shown using thin-layer approximations to the Navier-Stokes equations. The pressure contours show the compression and expansion waves downstream of the shock impingement, which are caused by the interaction of the incoming shock wave with the separated boundary layer.
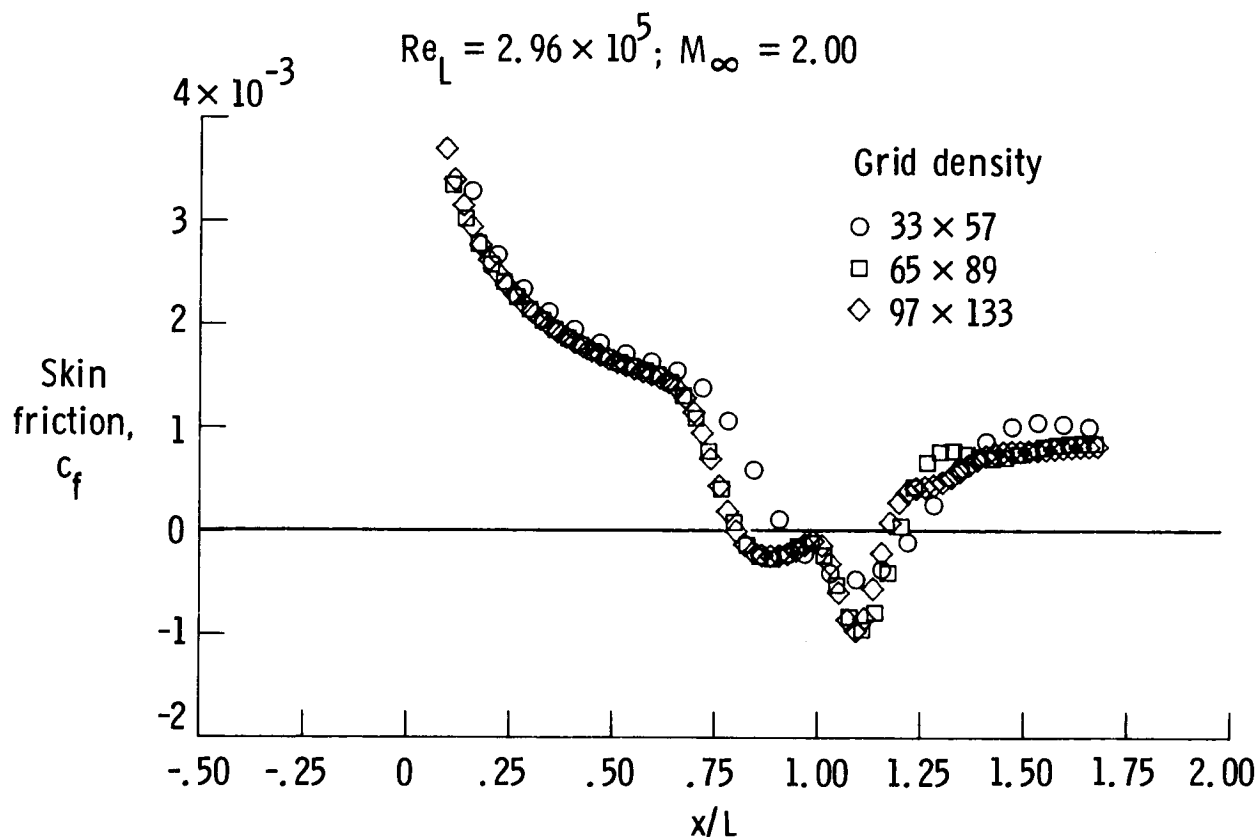
$$Re_L = 2.96 \times 10^5; \ M_\infty = 2.00$$

x/L
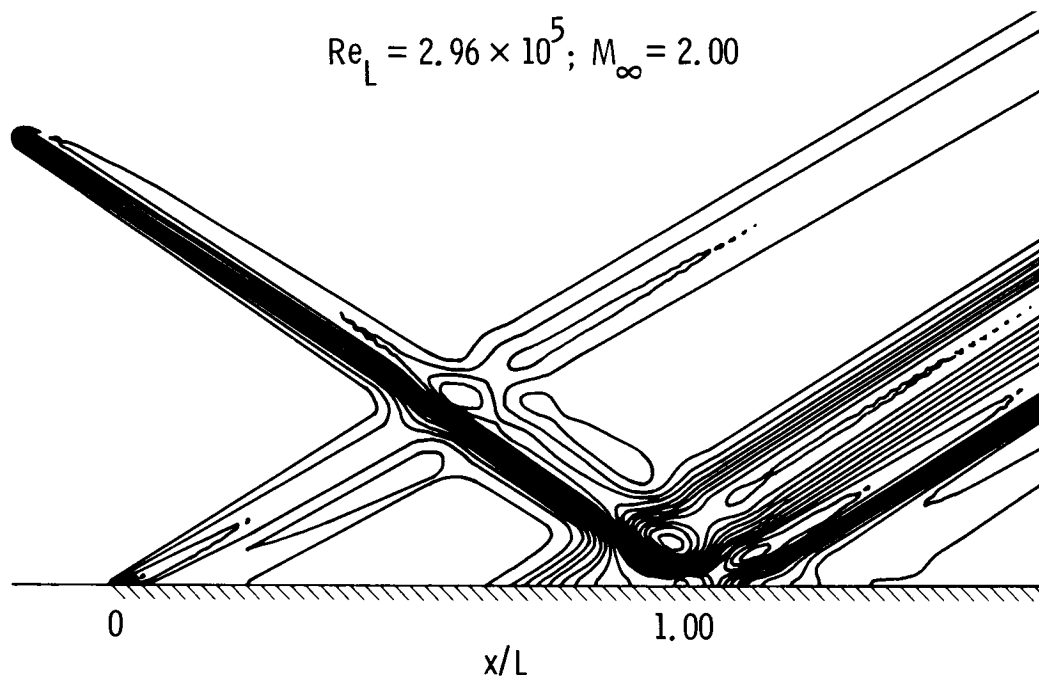
In order to assess the accuracy of the present upwind method, results from a grid convergence study are shown. Mesh densities two and three times the original grid were used. Details of the separated flow region are generally resolved with the second mesh, although a small difference exists between the second and third meshes near reattachment. Outside the separated flow region, very little difference in wall pressure exists in the results shown. The details in the present calculations clearly show the pressure plateau in the separation region.

$$Re_L = 2.96 \times 10^5; \ M_\infty = 2.00$$

Grid density

○ 33 × 57
□ 65 × 89
◇ 97 × 133

Wall pressure, p_{wall}/p_∞

104
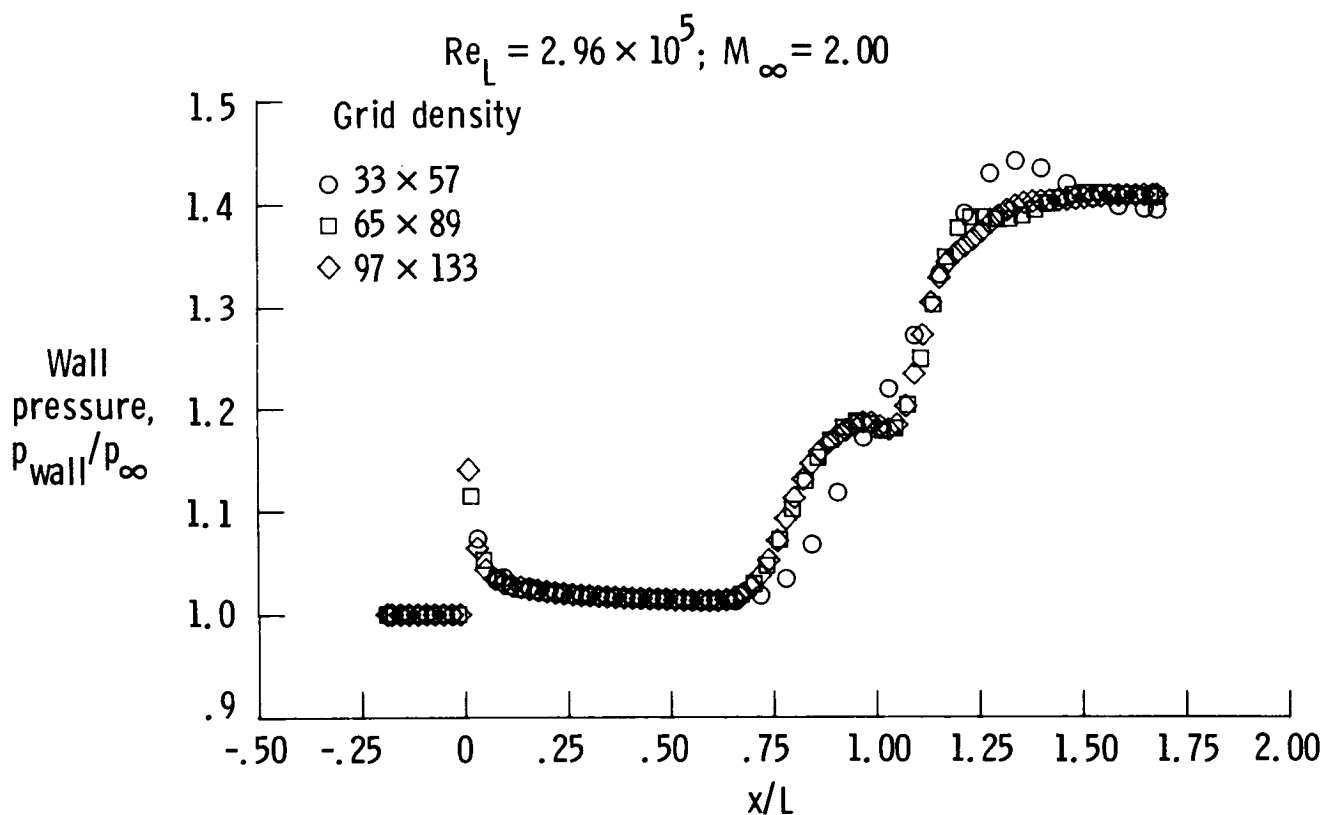
Shock-Boundary Layer Interaction: Skin Friction Coefficient

The skin friction coefficient predicted with the present method for the three meshes is shown. The skin friction exhibits three local extremum, two minimums and one maximum, in the separation zone. The separation extends from approximately 0.75 to 1.20 reference lengths from the leading edge of the plate.

$$Re_L = 2.96 \times 10^5; \quad M_\infty = 2.00$$

Skin friction, c_f

4×10^{-3}

Grid density

○ 33 × 57
□ 65 × 89
◇ 97 × 133

x/L

A comparison of wall pressure and skin friction from the present results with experiment is shown. The pressure plateau and the extent of separation are closely predicted. The arrows in the figure indicate that only the presence of separation was deduced from the experiment; the actual level of skin friction in the separation was not measured.

$$Re_L = 2.96 \times 10^5; \quad M_\infty = 2.00$$

Skin friction, c_f

Wall pressure, p_{wall}/p_∞

○   Experiment
—— Thin-layer Navier-Stokes

x/L
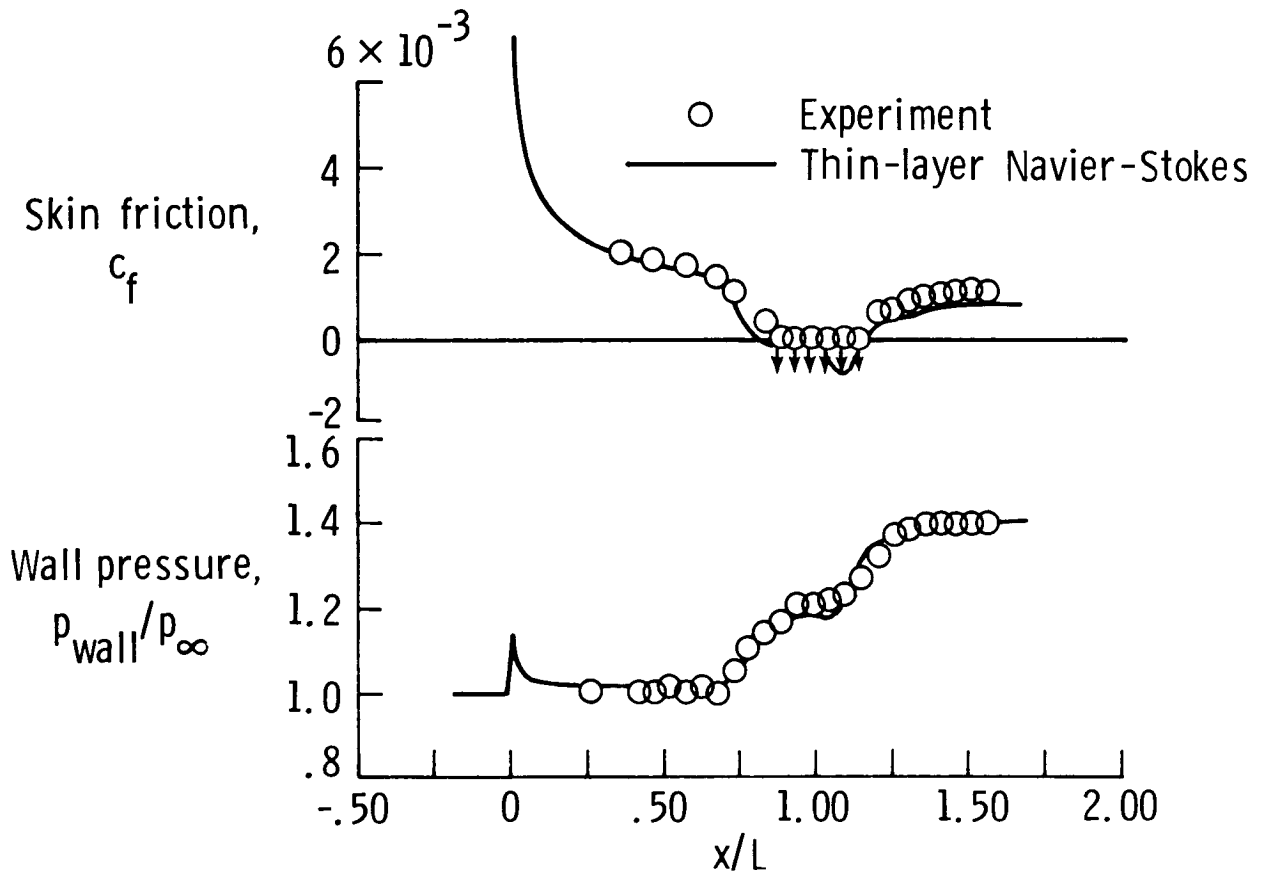
Concluding Remarks

Efficient solutions to steady-state Euler and Navier-Stokes equations are possible through the upwind relaxation algorithms discussed previously. The methods recover conventional space marching methods for fully supersonic flows and can be shown to be unconditionally stable in three dimensions. Accurate solutions to several inviscid and viscous model problems, including flat-plate boundary layer flow and shock/boundary layer interaction with separation, have been demonstrated. The method is currently being implemented in three dimensions.

Efficient solutions to steady-state equations possible through upwind relaxation

    Recovers space marching method for supersonic flows
    Unconditionally stable in three dimensions

Accurate solutions to several viscous flows demonstrated using second/third-order upwind differencing for convective and pressure terms

    Flat plate boundary layer
    Shock/boundary-layer interaction with separation